



Article

Enhancing the Microhardness of Coatings Produced by Cold Gas Dynamic Spraying through Multi-Reinforcement with Aluminum Powders Containing Fullerenes and Aluminum Nitride

Artemiy Aborkin ^{*}, Dmitry Babin, Leonid Belyaev and Dmitry Bokaryov

Department of Mechanical Engineering Technology, Vladimir State University Named after Alexander and Nikolay Stoletovs, Gorky Str. 87, 600000 Vladimir, Russia; necros-m2@yandex.ru (D.B.); blv_vlsu@mail.ru (L.B.); bokarev.1998@list.ru (D.B.)

* Correspondence: aborkin@vlsu.ru

Abstract: Coatings with high hardness were successfully obtained using low-pressure cold spray (LPCS) technology from nanocrystalline powders based on the aluminum alloy AlMg6, which were multi-reinforced with 0.3 wt.% fullerenes and 10–50 wt.% AlN. The powders were synthesized through a two-stage high-energy ball milling process, resulting in a complex mechanical mixture consisting of agglomerates and micro-sized ceramic particles of AlN. The agglomerates comprise particles of the nanocomposite material AlMg6/C₆₀ with embedded and surface-located, micro-sized ceramic particles of AlN. Scanning electron microscopy and EDS analyses demonstrated a uniform distribution of reinforcing particles throughout the coating volume. An X-ray diffraction (XRD) analysis of the coatings revealed a change in the predominant orientation of matrix alloy grains to a more chaotic state during deformation over the course of cold gas dynamic spraying. A quantitative determination of AlN content in the coating was achieved through the processing of XRD data using the reference intensity ratio (RIR) method. It was found that the proportion of transferred ceramic particles from the multi-reinforced powder to the coating did not exceed ~65%. Experimental evidence indicated that LPCS processing of mono-reinforced nanocrystalline powder composite AlMg6/C₆₀ practically did not lead to the formation of a coating on the substrate and was limited to a monolayer with a thickness of ~10 μm. The microhardness of the monolayer coating obtained from the deposition of AlMg6/C₆₀ powder was 181 ± 12 HV. Additionally, the introduction of 10 to 50 wt.% AlN into the powder mixture contributed to the enhancement of growth efficiency and an increase in coating microhardness by ~1.4–1.7 times. The obtained results demonstrate that the utilization of agglomerated multi-reinforced powders for cold gas dynamic spraying can be an effective strategy for producing coatings and bulk materials based on aluminum and its alloys with high microhardness.



Citation: Aborkin, A.; Babin, D.; Belyaev, L.; Bokaryov, D. Enhancing the Microhardness of Coatings Produced by Cold Gas Dynamic Spraying through Multi-Reinforcement with Aluminum Powders Containing Fullerenes and Aluminum Nitride. *J. Manuf. Mater. Process.* **2023**, *7*, 203. <https://doi.org/10.3390/jmmp7060203>

Academic Editor: Shuo Yin

Received: 22 October 2023

Revised: 14 November 2023

Accepted: 15 November 2023

Published: 18 November 2023

Keywords: multi-reinforcement; aluminum nitride; fullerenes; cold spraying; aluminum matrix composites



Copyright: © 2023 by the authors. Licensee MDPI, Basel, Switzerland. This article is an open access article distributed under the terms and conditions of the Creative Commons Attribution (CC BY) license (<https://creativecommons.org/licenses/by/4.0/>).

1. Introduction

One of the promising methods that can be effectively employed for creating coatings and bulk materials with tailored properties is the cold gas dynamic spraying (CGDS) method, characterized by a broad range of functional applications that encompass both protective coating deposition and surface restoration and offer prospects in the field of additive manufacturing [1]. Moreover, the flexibility of cold spray additive manufacturing enables the functionalization of several surfaces for various applications with various opportunities for material hybridizing, e.g., oxide/ceramic, oxide/polymer, metal/polymer, metal/PMCs, polymer/metal, metal/ceramic, ceramic/metal, and cermet/metal [2–4].

Aluminum-based powders, due to their high corrosion resistance, are in demand in the field of mechanical engineering for CGDS on machine components' surfaces. However, the primary drawbacks of aluminum and its alloy-based powder coatings, which hinders their wider application, are its low wear resistance and mechanical properties. These shortcomings are addressed through the development of composite coatings that are achieved by reinforcing aluminum powders with ceramic microparticles such as SiC [5,6], Al₂O₃ [7], B₄C [8–10], ZrO₂ [11], diamonds [12], and nanoparticles such as B₄C [10], TiB₂ [13], and nanodiamonds [14,15].

The advantages of using ceramic microparticles for reinforcing aluminum lie in their relatively low cost and the high deposition efficiency of such mixtures, ensuring a high transfer rate of ceramic particles into the coating and the consequent enhancement of its hardness. However, the drawback is the relatively low microhardness of the coating, which usually does not exceed 200 HV when the ceramic particle content is around 40 vol.% and often falls lower around 100–150 HV [16,17]. Coatings with a greater nanohardness of 3.02 GPa were achieved by Woo et al. [14] during gas dynamic spraying of aluminum powder reinforced with 10 wt.% nanodiamonds (NDs). Furthermore, in their study [14], it was noted that increasing the ball milling time of the ND–Al powder composite from 0.5 to 3 h led to a decrease in the deposition efficiency of the coating from 14.2% to 3.8%. This was attributed to the increased hardness of the powder particles due to prolonged ball milling, as harder particles require more kinetic energy for compaction and, consequently, a higher critical velocity [18]. This renders the use of such powder blends for LPCS deposition either inefficient or impractical. Another issue associated with CGDS of polydisperse powder mixtures containing nanoscale reinforcement particles is the high instability of nanoparticles in the gas stream [19,20]. This can lead to a significant dispersion of nanoscale particles during deposition, preventing their effective transfer into the coating. Therefore, it is advisable to utilize agglomerated powders obtained, for example, through high-energy ball milling [16]. In this case, the reinforcing nanoparticles are embedded inside matrix powder particles, forming agglomerates that minimize their loss during CGDS [21].

Considering the experience in creating bulk composites based on aluminum and its alloys, the use of carbon nanostructures, such as fullerenes [22–24], appears promising for enhancing microhardness. For instance, Evdokimov et al. [22] produced bulk composites based on the AlMg6 alloy that were reinforced with C₆₀ fullerenes through high-energy planetary ball milling followed by hot extrusion. The microhardness of the composite material reinforced with 0.3 wt.% fullerenes reached 220 HV. Nam et al. [23] reported that the maximum hardness values for Al matrix composites reinforced with 5 vol.% C₆₀ fullerenes after annealing at 500 °C were 250 HV. Improving the deposition efficiency of agglomerated powders reinforced with nanoparticles can be achieved by introducing ceramic microparticles into the powder blend [25]. This is because both asperity creation and oxide layer removal mechanisms significantly influence the increase in deposition efficiency [26]. AlN microparticles, considering their low coefficient of thermal expansion, excellent wear resistance, and corrosion resistance, are a promising reinforcement for aluminum matrix composites, providing enhanced structural and functional properties [27].

Thus, this study is dedicated to enhancing the microhardness of coatings obtained through low-pressure gas dynamic spraying by employing multi-reinforcement of aluminum powders with fullerenes and aluminum nitride. To achieve this, we synthesized powder blends based on the AlMg6 aluminum alloy, multi-reinforced with 0.3 wt.% fullerenes and 10–50 wt.% AlN, using a two-stage high-energy milling method. Extensive characterization of the synthesized powder mixtures, including scanning electron microscopy and X-ray diffraction, was conducted to examine their structure, phase composition, and particle size distribution. Subsequently, the obtained powders were sprayed onto steel substrates using the low-pressure gas dynamic spraying method. The microstructure and phase composition of the formed coatings were then studied, and quantitative assessments of the transfer of ceramic particles from the powder mixture to the coating were conducted. The influence of ceramic microparticle content on the enhancement of

growth efficiency and microhardness of the coatings was investigated. Finally, a comparison of the microhardness of the obtained coatings was conducted using known data from the literature.

2. Materials and Methods

Multi-reinforced powders for CGDS were prepared through a two-stage ball milling process of the initial components. Figure 1 illustrates a schematic representation of the multi-reinforced powder production process.

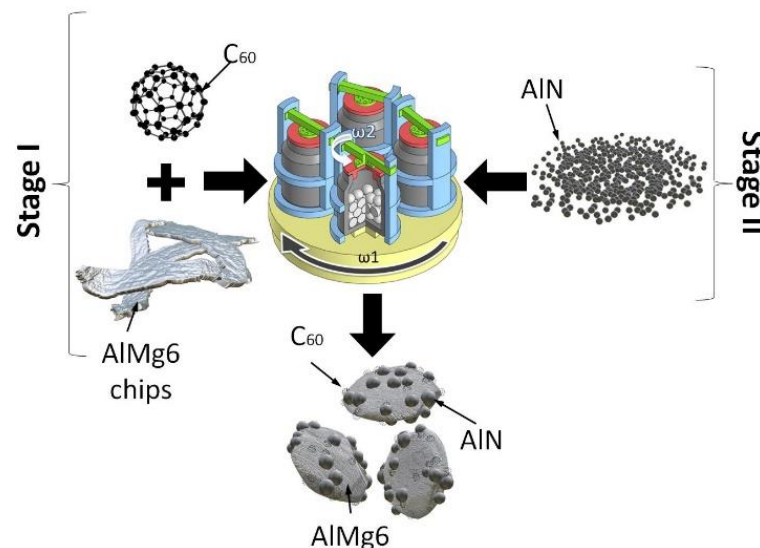


Figure 1. Schematic representation of the two-stage route for producing multi-reinforced powders.

At the first stage, a composite nanostructured powder based on the aluminum alloy AlMg6, reinforced with C60 fullerenes, was obtained. For this purpose, high-energy ball milling was performed on AlMg6 alloy shavings with the addition of 0.3 wt.% C60 fullerenes using a planetary mill AGO-2U. The mixture was processed in a steel milling container with steel balls of 8 mm in diameter at a rotational speed of 1800 rpm for 60 min with a powder-to-ball mass ratio of 1:20. High-energy ball milling was carried out in cycles of 5 min each with 3 min pauses to maintain the necessary thermal process regime. The second stage involved the simultaneous processing of the obtained nanocomposite powder AlMg6/C60 and ceramic AlN particles. For this purpose, the nanocomposite powder AlMg6/C60 was placed in a ZrO₂ container, and 10, 30, or 50 wt.% spherical AlN particles with an average size of 5.9 μm (see Figure 2a) were added. The mixtures were subjected to ball milling at a rotational speed of 600 rpm for 15 min using ZrO₂ balls with 8 mm diameters in a FRITSCH PULVERISETTE 6 planetary mill.

Coatings from the obtained multi-reinforced powders were formed using the cold gas dynamic spraying method at low pressure. The DIMET-404 setup was employed for this purpose. The selection of spray parameters was guided by the findings of previous studies [21,25]. Deposition was carried out onto 08 kp steel substrates. Air with a pressure of 0.8 MPa served as the working gas, with an air flow temperature of 450 °C. Spraying was performed in a stationary mode, i.e., without nozzle movement. The powder feed exposure time was set at 15 s. The distance from the nozzle orifice to the substrate surface was 10 mm. As a result, coatings of varying heights in the form of cones were obtained, depending on the composition of the powder mixture. The height of the cones (coating thickness) was measured using a micrometer.

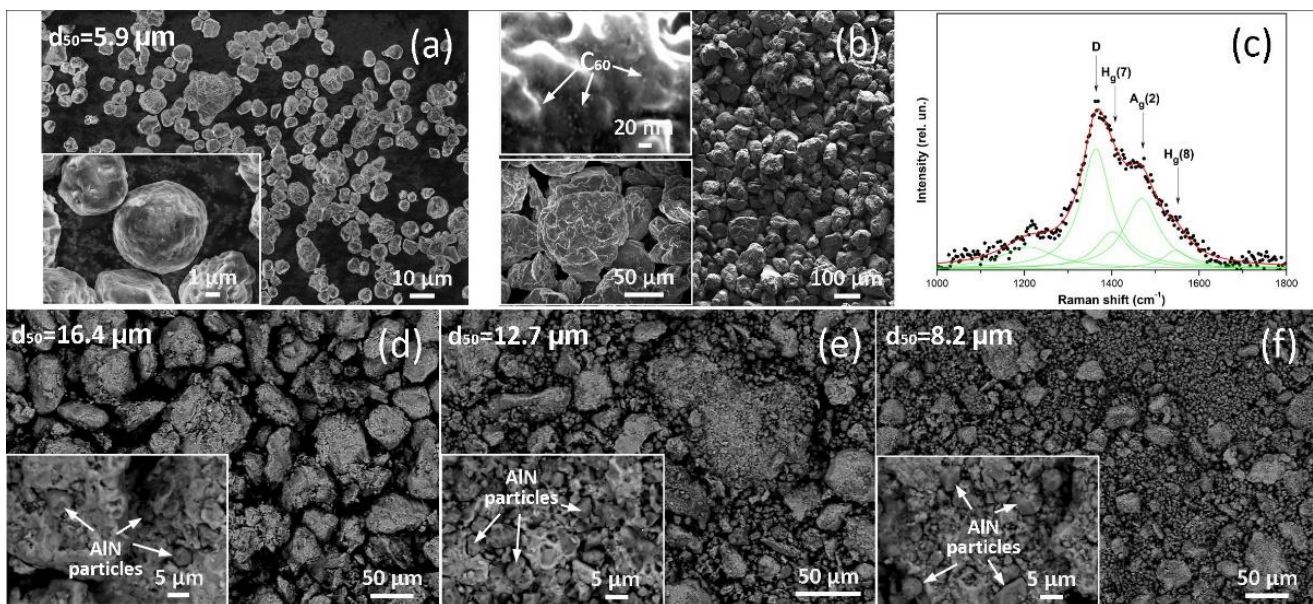


Figure 2. SEM images of the original AlN particles (a); the composite powder AlMg6/C₆₀ obtained after the first stage of ball milling (b); the Raman spectrum of the composite powder AlMg6/C₆₀ obtained after the first stage of ball milling (c); SEM images of the multi-reinforced powder with 10 wt.% AlN (d); the multi-reinforced powder with 30 wt.% AlN (e); and the multi-reinforced powder with 50 wt.% AlN (f).

The particle size distribution of the obtained multi-reinforced powders was determined using the Microsizer-201C analyzer. The surface morphology of the powders synthesized in the first stage was characterized using a Zeiss Ultra plus high-resolution field emission scanning electron microscope based on the Ultra 55. The composite powder AlMg/C₆₀ was also investigated using Raman spectroscopy on an Integra Spectra system at 473 nm with a power not exceeding 50 mW. Combination light scattering spectra were measured at more than 10 different points. Deconvolution of the obtained spectra was performed using a Lorentzian function. The multi-reinforced powders obtained in the second stage, as well as the coatings deposited from them, were examined using a scanning electron microscope LEO 1450 VP equipped with an INCA 300 energy-dispersive X-ray spectroscopy (EDS) detector. The structural and phase composition of the powders and resulting coatings were analyzed using X-ray diffraction on a D8 ADVANCE instrument. The well-established reference intensity ratio (RIR) method was employed for the quantitative determination of AlN content in the coating. Quantitative analysis of AlN content was performed by processing XRD data using DIFFRAC.EVA v2.0 software with ICDD PDF2. The crystallite size of the matrix alloy for both powders and coatings were calculated using the Scherrer equation. The volume-averaged crystallite sizes were calculated under the assumption of a spherical shape.

The microhardness of the coatings was measured on cross-sectioned samples using the Vickers method with a Shimadzu HMV-2 tester at a load of 245 mN and a dwell time of 10 s. A minimum of 10 measurements were performed for each sample.

3. Results and Discussion

Figure 2b shows typical SEM images of the composite powder AlMg6/C₆₀ obtained in the first stage of ball milling. Additionally, the insets depict magnified fragments of the powder particle surfaces. In this case, the powder mixture consisted of particles (agglomerates) with a size not exceeding 300 μm , comprising the matrix alloy AlMg6 and fullerenes. The particles (agglomerates) exhibit a rounded shape with a well-developed surface (see the inset in the lower left corner of Figure 2b). At higher magnification (see the inset in the

upper left corner of Figure 2b), a uniformly distributed reinforcement on the surface of the powder particles was observed. According to the SEM image, this reinforcement appears to be agglomerates of C_{60} fullerene molecules with a size of approximately 3–5 nm.

Figure 2c presents the typical Raman spectroscopy data of the AlMg6/ C_{60} composite powder obtained after the first stage of processing. Due to the low concentration and sufficiently good dispersion of C_{60} particles in the powder blend, as observed in SEM images (see inset in Figure 2b), and due to the presence of a background signal generated by the matrix material, it is challenging to identify C_{60} lines in the Raman spectrum. Nevertheless, signal deconvolution revealed lines around $\sim 1403\text{ cm}^{-1}$, $\sim 1469\text{ cm}^{-1}$, and $\sim 1549\text{ cm}^{-1}$, characteristic of fullerene dimers and 2D polymeric networks. For instance, the presence of Ag(2) serves as an excellent indicator of C_{60} polymerization [28]. Additionally, the spectrum exhibits the D-line, originated by the breathing mode of defective sp²-hybridised aromatic C-C rings around $\sim 1364\text{ cm}^{-1}$.

Figure 2d–f shows SEM images of the multi-reinforced powder mixtures with 10, 30, or 50 wt.% AlN, which were obtained after the second stage of ball milling.

The insets also show magnified fragments of the powder particle surfaces. Analysis of the SEM images of multi-reinforced powders with different AlN content demonstrates their differences. For instance, in the mixture with 10 wt.% AlN, a small number of free ceramic particles is noticeable. In this case, the AlN particles are almost entirely distributed on the surface of the AlMg6 matrix alloy or embedded within it (see Figure 2d). However, for compositions containing 30 or 50 wt.% AlN (see Figure 2e,f), a different pattern emerges. A significant number of free ceramic particles in the powder mixture is observed, which increases with the rise in AlN content. This suggests the presence of a certain “saturation threshold” at which the surface of the matrix alloy particles is almost entirely covered by solid ceramic inclusions. This either prevents or at least hinders the incorporation of AlN into the ductile matrix alloy. Additionally, the surface of the matrix alloy particles becomes more developed, which is attributed to the deformational impact of ceramic particles during ball milling. Submicron- and micron-sized particles of the matrix material are formed through the micro-cutting of the relatively harder ceramic particles on the surface of the matrix alloy particles.

It is worth noting that the incorporation of ceramic particles facilitates the penetration of C_{60} molecule agglomerates from the surface into the interior of the matrix alloy particles. A comprehensive analysis of the particle size distribution and SEM images of the powders in Figure 2b,d–f shows a reduction in the particle sizes of the AlMg6 matrix after the second stage of processing. Moreover, the increase in AlN content from 10 to 50 wt.% also leads to a decrease in d_{50} in the powder mixture, decreasing from 16.4 to 8.2 μm . On the one hand, this is undoubtedly related to the influence on measurement results of the higher proportion of finer AlN particles, where d_{50} is 5.9 μm . On the other hand, the presence of AlN on the surface of AlMg6 matrix alloy particles hinders the welding processes between them and intensifies the dispersion processes during ball milling.

Thus, the obtained multi-reinforced powders represent a complex mechanical mixture consisting of agglomerates and microparticles of ceramic AlN. The agglomerates consist of particles of the nanocomposite material AlMg6/ C_{60} with embedded and surface-located ceramic AlN microparticles. Moreover, the concentration of AlN particles on the surface of the agglomerates and within their volume increased with the growth of the weight fraction of ceramic particles in the initial mixture.

The results of the XRD analysis for the powders obtained after the first and second stages of ball milling are shown in Figure 3a.

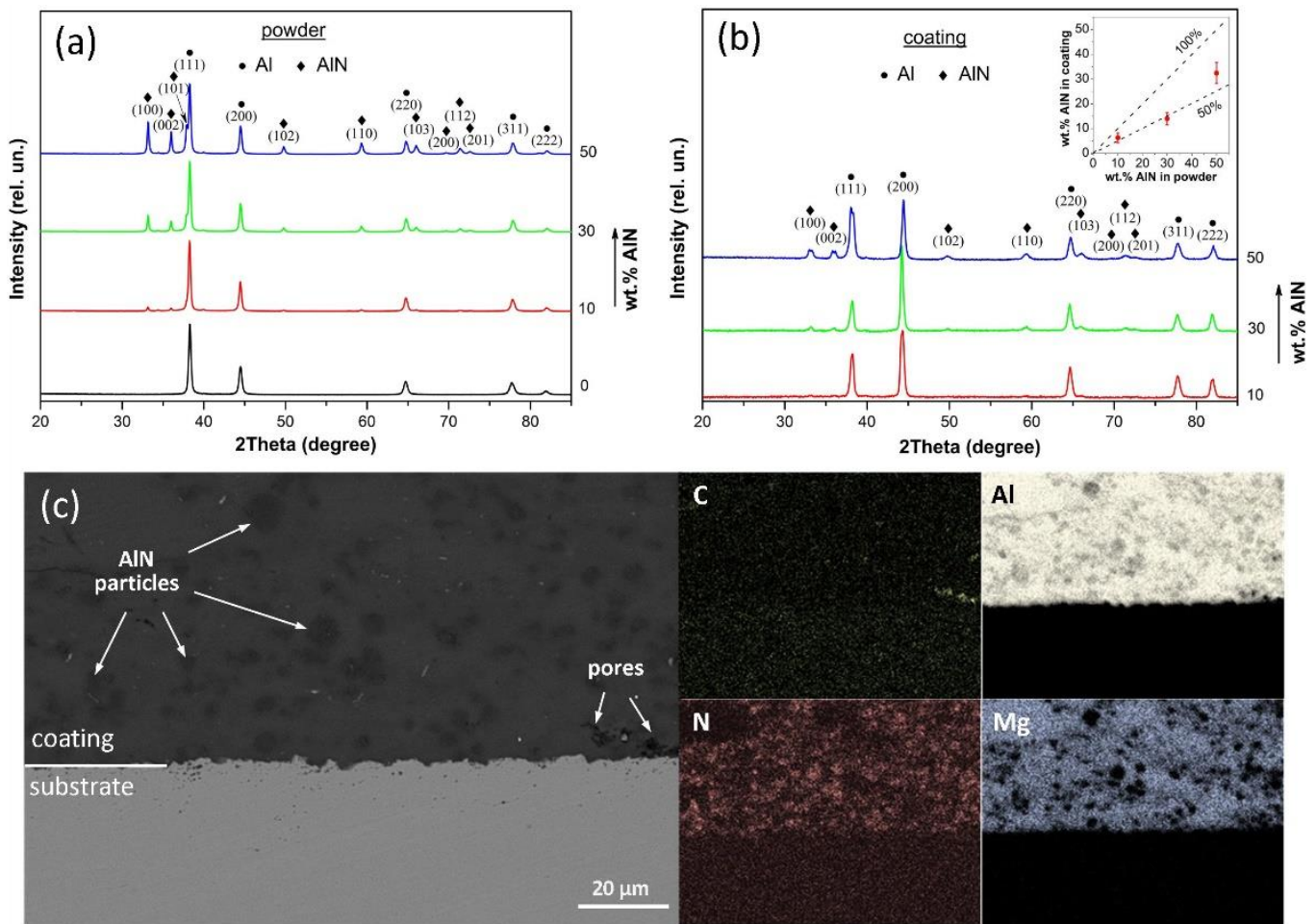


Figure 3. XRD of mechanically synthesized, multi-reinforced powder mixtures with different amounts of ceramic particles (a); XRD of coatings (b); SEM image of the cross-section of the coating AlMg6/C₆₀ + 30 wt.% AlN with EDS mapping (c).

For the powders obtained at the first stage, distinct (111), (200), (220), (311), and (222) peaks of aluminum were clearly observed. However, no diffraction peaks of the reinforcing phase C₆₀ were detected. This can be attributed to the low content of C₆₀ in the powder mixture and may also be explained by the X-ray radiation micro-absorption during the X-ray phase analysis of composites reinforced with well-dispersed carbon nanostructures [29]. This is a typical observation for aluminum alloys reinforced with carbon structures, particularly at higher concentrations of reinforcing additives [30,31]. XRD data for the multi-reinforced powders obtained at the second stage show a qualitatively similar character. In this case, in addition to peaks corresponding to the matrix alloy, peaks of aluminum nitride (AlN) are also identified. The intensity of the AlN peaks increases with a higher content of AlN in the powder mixture. Based on the full width at half maximum (FWHM) of the matrix alloy peaks, the crystallite size was calculated. The crystallite size of the matrix alloy calculated for the composite powder AlMg6/C₆₀ obtained at the first stage of ball milling was approximately ~60 nm. After the second stage of ball milling, the crystallite size of the matrix alloy was approximately ~40–60 nm. This corresponds to the crystallite size of aluminum-based powders reinforced with 10 wt.% nanodiamonds after 3 h of ball milling [14]. This allows us to predict the formation of a nano- or submicrocrystalline structure in coatings produced from these powders.

Figure 3b shows XRD data for coatings formed from multi-reinforced powders through the CGDS method. It is noteworthy that the formation of coatings with a thickness exceeding approximately 10 μm from the powder mixture obtained in the first stage of ball

milling (without ceramic particles) was not achieved. This limitation can be attributed to both the temperature and velocity constraints imposed by the utilized spray system and the powder particle size. Therefore, the XRD data in Figure 3b are presented solely for powder mixtures containing 10, 30, or 50 wt.% AlN. The XRD data obtained for powders and coatings exhibit some differences. For instance, a reduction in the peak signal (111) of the aluminum crystalline plane (see Figure 3b) is observed in coatings compared with powders (Figure 3a), indicating a diminished proportion of crystalline planes (111). This suggests a change in the preferred orientation of grains in the matrix alloy towards a more chaotic arrangement during the CGDS process. Additionally, the intensity of peaks corresponding to the ceramic phase of the coating is slightly lower than that in the powders, indicating an incomplete transfer of ceramic particles from the powder mixture to the coating. To assess the AlN content in the formed coatings, a quantitative analysis was performed. The inset in Figure 3b presents data on the AlN content in the coating as a function of the AlN content in the powder. For instance, when using a powder mixture containing 10 wt.% AlN, the AlN content in the coating was 6.3 ± 1.8 wt.%. Increasing the AlN content in the powder mixture from 30 to 50 wt.% raised its content in the coating from 14.1 ± 2.5 wt.% to 32.4 ± 4.2 wt.%. Thus, according to the quantitative XRD analysis under the applied conditions of CGDS, the proportion of transferred ceramic particles into the coating did not exceed ~65% and reached a minimum value of ~47% for the 30 wt.% AlN composition. However, this is a favorable result, as in previous studies [32–34], the transfer ratio of ceramic reinforcing particles into the coating did not exceed 50%. On the contrary, the authors of [34,35] were able to achieve a 100% transfer of ceramic reinforcing particles into the coating for some powder mixture compositions. The calculation of the crystallite size of the matrix alloy after coating deposition yielded values of approximately 80–120 nm, indicating that the nanocrystalline structure achieved during high-energy ball milling is largely retained during the spraying process. This aligns with the findings of [36–38] and allows for the prediction of a high microhardness of the obtained coatings due to grain boundary strengthening of the matrix alloy.

The coatings exhibit a relatively homogeneous microstructure, consisting of densely packed deformed particles of the matrix alloy with uniformly distributed carbon nanostructures and ceramic particles throughout their volume. Figure 3c presents a typical SEM image of coatings reinforced with 0.3 wt.% C₆₀ and 30 wt.% AlN along with EDS mapping data. Occasional pores were observed within the body of the coating, with sizes not exceeding ~8–10 μm. This allows for a qualitative assessment of the low porosity of the coatings. Thus, the analysis of SEM images of the coating microstructure leads to the conclusion that under the employed temperature–speed deposition conditions, the kinetic energy for the particle compaction of the matrix alloy remains sufficient for the effective formation of coatings with low porosity despite the formation of a nanocrystalline structure in the AlMg6 matrix alloy. Furthermore, it is worth noting that there is a minor alteration in the microgeometry of the substrate during the CGDS process, which is attributed to the erosive impact of the sprayed powder mixture on the substrate.

In the inset of Figure 4, macrograph images are presented, depicting cone-shaped coatings of varying heights. As previously mentioned, the deposition of a monodispersed powder composite scarcely resulted in the formation of a coating on the substrate and was confined to a monolayer.

A comparative analysis of the heights of formed cones reveals that an increase in AlN content in the mixture from 10 to 30 wt.% contributes to an approximately 19% increase in cone height achieved during the same deposition time, increasing from 4.7 to 5.8 mm. A further increase in the AlN content in the mixture to 50 wt.% results in a decrease in cone height to 5.5 mm. This may be attributed to the predominance of erosion processes by ceramic particles as well as a reduction in the particle size of the powder composition. Figure 4 also presents the results of microhardness measurements of coatings with varying AlN content in the powder mixture. For instance, the microhardness of a single-layer coating obtained by depositing AlMg6/C₆₀ powder was 181 ± 12 HV. Increasing the C₆₀

content is likely to lead to additional microhardness enhancement, but it may affect the coating growth efficiency negatively. The optimal C_{60} content for this purpose requires further investigation as varying the powder composition and deposition temperature–speed conditions can be utilized to control both the coating properties and its growth efficiency. The incorporation of AlN into the powder composition from 10 to 50 wt.% has led to an increase in the microhardness of the coatings from 259 ± 10 to 306 ± 12 HV. Comparing the microhardness data of mono- and multi-reinforced powders allows us to conclude that the high microhardness of the coating is primarily achieved through the elevated microhardness of the AlMg6/ C_{60} nanocomposite material and secondarily due to the presence of hard ceramic microparticles of AlN in the forming coating. It is evident that the microhardness of AlMg6/ C_{60} is significantly influenced by grain boundary strengthening, which is dependent on the grain size of the AlMg6 matrix alloy and is described by the Hall–Petch relationship. Simultaneously, nanoscale particles primarily enhance the microhardness of the aluminum matrix, impeding dislocation movement; i.e., Orowan strengthening is realized. While all these factors positively contribute to the increased microhardness of the coatings, they adversely affect their growth capability. The presence of C_{60} in the aluminum alloy restricts the deformation of the matrix material or at the very least demands greater kinetic energy for particle compaction.

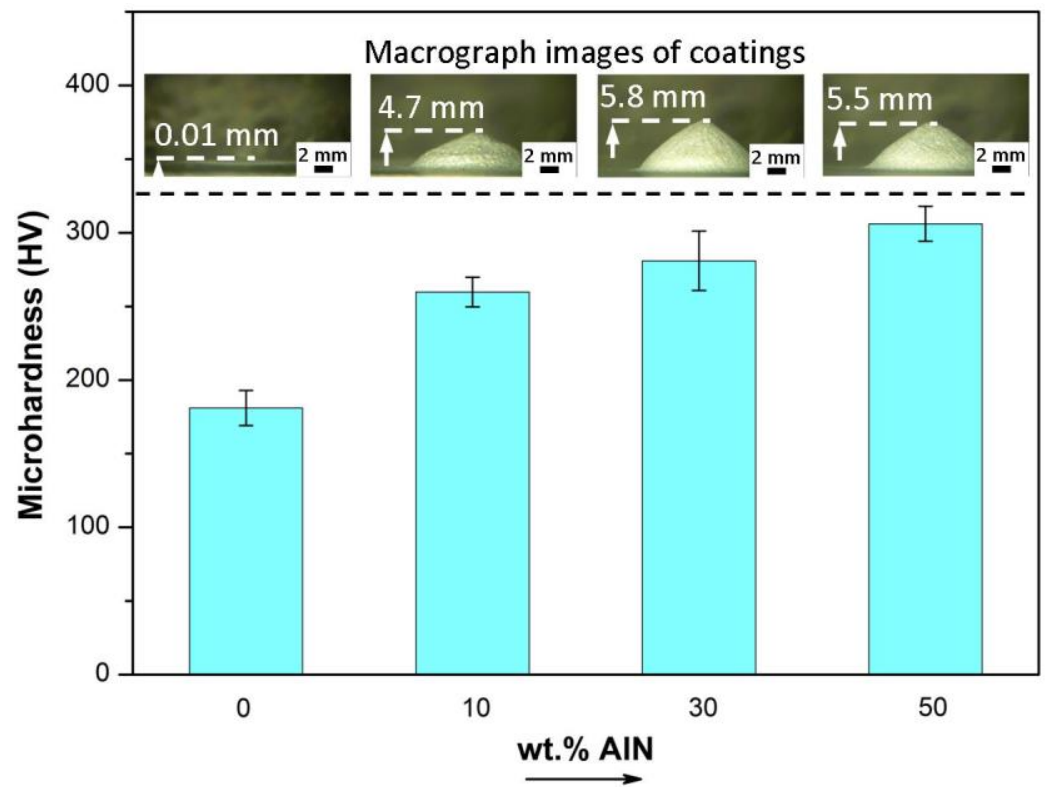


Figure 4. Effect of AlN content on the microhardness of the coating. The inset shows macrograph images of the sprayed coating along with their respective height measurements.

Figure 5 shows the summary data reflecting the dependence of the change in microhardness of the coating based on aluminum and its alloys on the content of reinforcing ceramic particles.

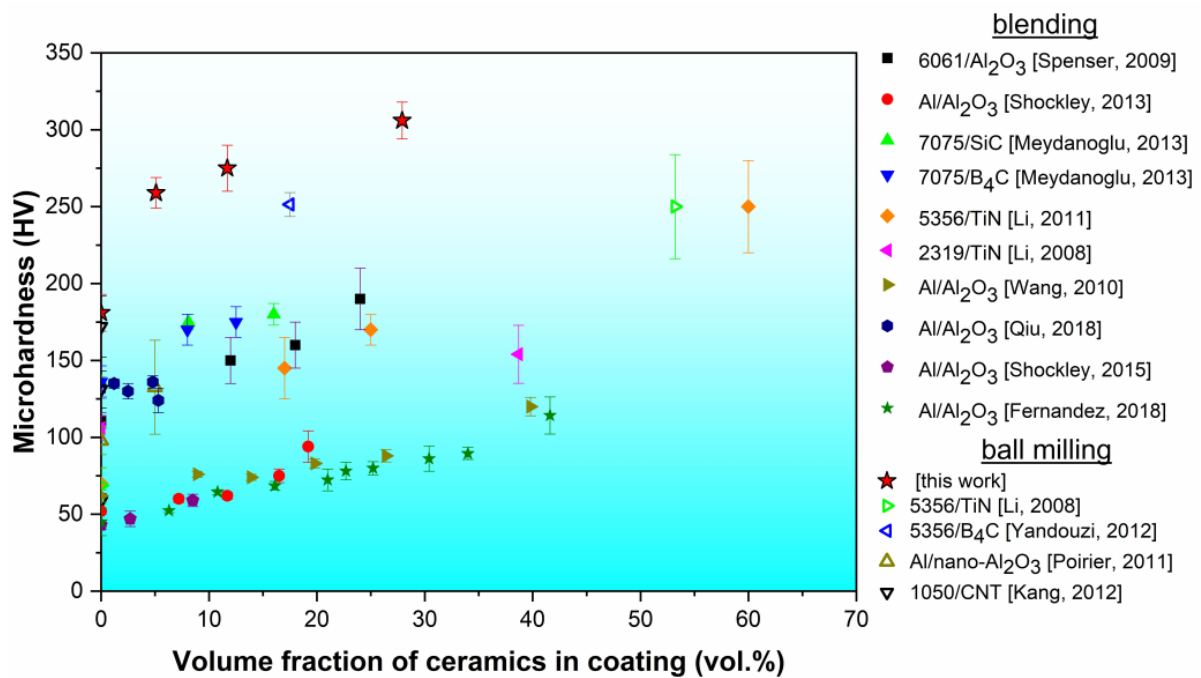


Figure 5. Dependence of microhardness of cold sprayed coatings based on aluminum and its alloys on the volume fraction of reinforcing ceramic particles in the coating [26,32,35,39–47].

A comparative analysis shows that the multi-reinforced coatings obtained in this work provide the best microhardness values among other powder compositions based on aluminum and its alloys used for cold gas dynamic spraying. This concerns the reinforcement of powder compositions with various nano- and microparticles, which were obtained both by simple mechanical mixing [26,32,35,39–43] and high-energy ball milling [44–47]. By analyzing the data presented in Figure 5, it is evident that the use of ball milling techniques for preparing composite powders generally allows for the production of powder mixtures that facilitate the formation of harder CGDS coatings. The hardness of coatings from composite powders obtained by blending techniques is slightly lower. This can be explained by the formation of a homogeneous structure of the composite material with ultra-dispersed grains of the matrix alloy during ball milling, effectively increasing the microhardness of the composite coating. However, in most cases, the successful deposition of such powder mixtures requires higher values of gas pressure or temperature. Conversely, multi-reinforced powder mixtures synthesized in this study were successfully deposited using the LPCS technology with air as the carrier gas. The presented results demonstrate that the use of multi-reinforced powders for CGDS can be an effective strategy for the formation of coatings and bulk materials based on aluminum and its alloys with high microhardness.

4. Conclusions

Through a two-stage high-energy ball milling process, powders based on the aluminum alloy AlMg6 that were multi-reinforced with fullerenes (0.3 wt.%) and aluminum nitride (10–50 wt.%) were synthesized. These powders represent a complex mechanical mixture comprising agglomerates and micro-sized ceramic particles of AlN. The agglomerates consist of particles of the nanocomposite material AlMg6/C₆₀ with embedded, as well as surface-located, micro-sized ceramic particles of AlN. The concentration of AlN ceramic particles on the surface of the agglomerates and within their volume increased with the increase in the weight fraction of ceramic particles in the initial mixture. The average particle size of the synthesized powders, depending on the ceramic concentration in the initial powder mixture, ranged from 8.2 to 16.4 μm. Cold gas dynamic spraying of multi-reinforced powders onto 1008 steel substrates was performed. It was demonstrated that the resulting coatings exhibit a relatively homogeneous microstructure with evenly

distributed reinforcing particles throughout their volume. According to the XRD data, the fraction of transferred ceramic particles into the coating did not exceed ~65%. Cold gas dynamic spraying of a mono-reinforced powder composite AlMg6/C₆₀ practically did not result in the formation of a coating on the substrate and was confined to a monolayer. The microhardness of the monolayer coating obtained by depositing AlMg6/C₆₀ powder was 181 ± 12 HV. The incorporation of AlN into the powder mixture from 10 to 50 wt.% contributed to an approximately 1.4–1.7 times increase in the microhardness of the coatings. A comparison of the microhardness of the obtained coatings with data from the literature reveals that these coatings exhibit superior microhardness performance when compared with other powder compositions based on aluminum and its alloys commonly used in cold gas dynamic spraying.

Author Contributions: Data curation, D.B. (Dmitry Babin), L.B. and D.B. (Dmitry Bokaryov); investigation, D.B. (Dmitry Babin), L.B. and D.B. (Dmitry Bokaryov); methodology, A.A.; project administration, A.A.; supervision, A.A.; writing—original draft, D.B. (Dmitry Bokaryov); writing—review and editing, A.A. All authors have read and agreed to the published version of the manuscript.

Funding: This research was carried out within the state assignment in the field of scientific activity of the Ministry of Science and Higher Education of the Russian Federation (theme FZUN-2020-0015, state assignment of VISU).

Data Availability Statement: The data presented in this study are available in this article.

Conflicts of Interest: The authors declare no conflict of interest.

References

1. Yin, S.; Cavaliere, P.; Aldwell, B.; Jenkins, R.; Liao, H.; Li, W.; Lupoi, R. Cold spray additive manufacturing and repair: Fundamentals and applications. *Addit. Manuf.* **2018**, *21*, 628–650. [\[CrossRef\]](#)
2. Raoulison, R.N.; Xie, Y.; Sapanathan, T.; Planche, M.P.; Kromer, R.; Costil, S.; Langlade, C. Cold gas dynamic spray technology: A comprehensive review of processing conditions for various technological developments till to date. *Addit. Manuf.* **2018**, *19*, 134–159. [\[CrossRef\]](#)
3. Perna, A.S.; Viscusi, A.; Gatta, R.D.; Astarita, A. Cold spraying on polymer-based composites: Understanding the single-particle adhesion. *Surf. Coat. Technol.* **2022**, *447*, 128837. [\[CrossRef\]](#)
4. Perna, A.S.; Viscusi, A.; Astarita, A.; Boccarusso, L.; Caraviello, A.; Carrino, L.; Durante, M.; Sansone, R. Experimental Study of Functionalized Polymer Matrix Composite with Multi-Material Metal Coatings Produced by Means of Cold Spray Technology. *Key Eng. Mater.* **2019**, *813*, 267–272. [\[CrossRef\]](#)
5. Gyansah, L.; Tariq, N.H.; Tang, J.R.; Qiu, X.; Feng, B.; Huang, J.; Du, H.; Wang, J.Q.; Xiong, T.Y. Cold spraying SiC/Al metal matrix composites: Effects of SiC contents and heat treatment on microstructure, thermophysical and flexural properties. *Mater. Res. Express.* **2018**, *5*, 026523. [\[CrossRef\]](#)
6. Kumar, S.; Reddy, S.K.; Joshi, S.V. Microstructure and performance of cold sprayed Al-SiC composite coatings with high fraction of particulates. *Surf. Coat. Technol.* **2017**, *318*, 62–71. [\[CrossRef\]](#)
7. Qiu, X.; Tariq, N.U.H.; Qi, L.; Tang, J.; Cui, X.; Wang, J.; Xiong, T. Influence of particulate morphology on microstructure and tribological properties of cold sprayed A380/Al₂O₃ composite coatings. *J. Mater. Sci. Technol.* **2020**, *44*, 9–18. [\[CrossRef\]](#)
8. Kosarev, V.F.; Klinkov, S.V.; Shikalov, V.S.; Chesnokov, A.E. A Study of the Neutron Absorbing Properties of Al + B₄C and Al + B Coatings Formed by Cold Gas-Dynamic Spraying. *Phys. Met. Metallogr.* **2023**, *124*, 308–314. [\[CrossRef\]](#)
9. Tariq, N.H.; Gyansah, L.; Wang, J.; Feng, B.; Siddiquee, M.T.; Xiong, T. Cold spray additive manufacturing: A viable strategy to fabricate thick B₄C/Al composite coatings for neutron shielding applications. *Surf. Coat. Technol.* **2018**, *339*, 224–236. [\[CrossRef\]](#)
10. Wu, C.; Lu, Y.; Luo, G.; Shen, Q.; Gan, Z.; Liu, J. Influence of particulate B₄C size on microstructural evolution and mechanical behavior in nanostructured Al matrix during heat treatment. *Powder Technol.* **2020**, *374*, 274–282. [\[CrossRef\]](#)
11. Martin, J.; Maizeray, A.; da Silva Tusch, C.; Marcos, G.; Czerwiec, T.; Henrion, G. A new strategy to prepare alumina-zirconia composite or multilayered coatings by combining cold-spray deposition and plasma electrolytic oxidation. *Mater. Today Commun.* **2023**, *36*, 106676. [\[CrossRef\]](#)
12. Chen, C.; Xie, Y.; Yan, X.; Ahmed, M.; Lupoi, R.; Wang, J.; Ren, Z.; Liao, H.; Yin, S. Tribological properties of Al/diamond composites produced by cold spray additive manufacturing. *Addit. Manuf.* **2020**, *36*, 101434. [\[CrossRef\]](#)
13. Chen, H.; Pala, Z.; Hussain, T.; McCartney, D. Fabrication and microstrain evolution of Al-TiB₂ composite coating by cold spray deposition. *Proc. Inst. Mech. Eng. L* **2019**, *233*, 1044–1052. [\[CrossRef\]](#)
14. Woo, D.J.; Heer, F.C.; Brewer, L.N.; Hooper, J.P.; Osswald, S. Synthesis of nanodiamond-reinforced aluminum metal matrix composites using cold-spray deposition. *Carbon* **2015**, *86*, 15–25. [\[CrossRef\]](#)

15. Loganathan, A.; Rengifo, S.; Hernandez, A.F.; Zhang, C.; Agarwal, A. Effect of nanodiamond reinforcement and heat-treatment on microstructure, mechanical and tribological properties of cold sprayed aluminum coating. *Surf. Coat. Technol.* **2021**, *412*, 127037. [[CrossRef](#)]
16. Xie, X.; Yin, S.; Raelison, R.; Chen, C.; Verdy, C.; Li, W.; Ji, G.; Ren, Z.; Liao, H. Al matrix composites fabricated by solid-state cold spray deposition: A critical review. *J. Mater. Sci. Technol.* **2021**, *86*, 20–55. [[CrossRef](#)]
17. Li, W.; Assadi, H.; Gaertner, F.; Yin, S. A Review of Advanced Composite and Nanostructured Coatings by Solid-State Cold Spraying Process. *Crit. Rev. Solid State Mater. Sci.* **2018**, *44*, 109–156. [[CrossRef](#)]
18. Jodoin, B.; Ajdelsztajn, L.; Sansoucy, E.; Zúñiga, A.; Richer, P.; Lavernia, E.J. Effect of particle size, morphology, and hardness on cold gas dynamic sprayed aluminum alloy coatings. *Surf. Coat. Technol.* **2006**, *201*, 3422–3429. [[CrossRef](#)]
19. Meyer, M.; Caruso, F.; Lupoi, R. Particle velocity and dispersion of high Stokes number particles by PTV measurements inside a transparent supersonic Cold Spray nozzle. *Int. J. Multiph. Flow.* **2018**, *106*, 296–310. [[CrossRef](#)]
20. Koithara, L.; Raelison, R.; Costil, S. Flow phenomenon of micron-sized particles during cold spray additive manufacturing: High-speed optic observation and characterization. *Adv. Powder Technol.* **2020**, *31*, 1060–1079. [[CrossRef](#)]
21. Aborkin, A.; Alymov, M.; Arkhipov, V.; Khrenov, D. Formation of Heterogeneous Powder Coatings with a Two-Level Micro- and Nanocomposite Structure under Gas-Dynamic Spraying Conditions. *Dokl. Phys.* **2018**, *63*, 50–54. [[CrossRef](#)]
22. Evdokimov, I.; Perfilov, S.; Pozdnyakov, A.; Blank, V.; Bagramov, R.; Perezhogin, I.; Kulnitsky, B.; Kirichenko, A.; Aksenenkov, V. Nanostructured Composite Materials Based on Al–Mg Alloy Modified with Fullerene C₆₀. *Inorg. Mater. Appl. Res.* **2018**, *9*, 472–477. [[CrossRef](#)]
23. Nam, S.; Lee, S.; Roh, A.; Son, H.; Kim, M.; Choi, H. Role of supersaturated Al–C phases in mechanical properties of Al/fullerene composites. *Sci. Rep.* **2021**, *11*, 13143. [[CrossRef](#)]
24. Reshetniak, V.; Reshetniak, O.; Aborkin, A.; Nederkin, V.; Filippov, A. Effect of the Interface on the Compressibility of Substances with Spherical Nano-Inhomogeneities on the Example of Al/C₆₀. *Nanomaterials* **2022**, *12*, 2045. [[CrossRef](#)]
25. Aborkin, A.; Arkhipov, V.; Sachkova, N.; Sychev, A.; Alymov, M. Effect of Al₂O₃ on the Microhardness of AMg₂/Graphite Nanocomposite Powder Gas Dynamic Coatings on Aluminum Alloys. *Met. Sci. Heat Treat.* **2019**, *61*, 360–365. [[CrossRef](#)]
26. Fernandez, R.; Jodoin, B. Cold Spray Aluminum–Alumina Cermet Coatings: Effect of Alumina Content. *J. Therm. Spray Technol.* **2018**, *27*, 603–623. [[CrossRef](#)]
27. Sun, X.; Hao, X.; Nie, J.; Fan, Y.; Chen, Y.; Liu, S.; Liu, X.; Zhao, Y. Microstructure and enhanced cryogenic tensile property of a heterostructured Al–AlN/Al–Mg composite fabricated by accumulative roll bonding (ARB). *J. Mater. Res. Technol.* **2022**, *21*, 532–545. [[CrossRef](#)]
28. Dorner-Reisel, A.; Ritter, U.; Moje, J.; Freiburger, E.; Scharff, P. Effect of fullerene C₆₀ thermal and tribomechanical loading on Raman signals. *Diam. Relat. Mater.* **2022**, *126*, 109036. [[CrossRef](#)]
29. Popov, V. X-ray micro-absorption enhancement for non-agglomerated nanodiamonds in mechanically alloyed aluminium matrix composites. *Phys. Status Solidi A* **2015**, *212*, 2722–2726. [[CrossRef](#)]
30. Aborkin, A.; Alymov, M.; Sobol'kov, A.; Khor'kov, K.; Babin, D. Effect of the Thermomechanical Treatment Conditions on the Consolidation, the Structure, and the Mechanical Properties of Bulk Al–Mg–C Nanocomposites. *Russ. Metall. Met.* **2018**, *7*, 625–632. [[CrossRef](#)]
31. Aborkin, A.; Alymov, M.; Kireev, A.; Elkin, A.; Sobol'kov, A. Mechanically Synthesized Composite Powder Based on AMg₂ Alloy with Graphite Additives: Particle Size Distribution and Structural-Phase Composition. *Nanotechnol. Russ.* **2017**, *12*, 395–399. [[CrossRef](#)]
32. Spencer, K.; Fabijanic, D.M.; Zhang, M.X. The use of Al–Al₂O₃ cold spray coatings to improve the surface properties of magnesium alloys. *Surf. Coat. Technol.* **2009**, *204*, 336–344. [[CrossRef](#)]
33. Qiu, X.; Wang, J.; Tang, J.; Gyansah, L.; Zhao, Z.; Xiong, T. Microstructure, microhardness and tribological behavior of Al₂O₃ reinforced A380 aluminum alloy composite coatings prepared by cold spray technique. *Surf. Coat. Technol.* **2018**, *350*, 391–400. [[CrossRef](#)]
34. Yandouzi, M.; Richer, P.; Jodoin, B. SiC particulate reinforced Al–12Si alloy composite coatings produced by the pulsed gas dynamic spray process: Microstructure and properties. *Surf. Coat. Technol.* **2009**, *203*, 3260–3270. [[CrossRef](#)]
35. Li, W.Y.; Yang, C.; Liao, H. Effect of vacuum heat treatment on microstructure and microhardness of cold-sprayed TiN particle-reinforced Al alloy-based composites. *Mater. Des.* **2011**, *32*, 388–394. [[CrossRef](#)]
36. Ajdelsztajn, L.; Schoenung, J.M.; Jodoin, B.; Kim, G. Cold spray deposition of nanocrystalline aluminum alloys. *Met. Mater. Trans. A Phys. Met. Mater. Sci.* **2005**, *36*, 657–666. [[CrossRef](#)]
37. Rokni, M.; Widener, C.; Nardi, A.; Champagne, V. Nano crystalline high energy milled 5083 Al powder deposited using cold spray. *Appl. Surf. Sci.* **2014**, *305*, 797–804. [[CrossRef](#)]
38. Hall, A.; Brewer, L.; Roemer, T. Preparation of aluminum coatings containing homogenous nanocrystalline microstructures using the cold spray process. *J. Therm. Spray Technol.* **2008**, *17*, 352–359. [[CrossRef](#)]
39. Shockley, J.; Strauss, H.; Chromik, R.; Brodusch, N.; Gauvin, R.; Irissou, E.; Legoux, J. In situ tribometry of cold-sprayed Al–Al₂O₃ composite coatings. *Surf. Coat. Technol.* **2013**, *215*, 350–356. [[CrossRef](#)]
40. Meydanoglu, O.; Jodoin, B.; Kayali, E.S. Microstructure, mechanical properties and corrosion performance of 7075 Al matrix ceramic particle reinforced composite coatings produced by the cold gas dynamic spraying process. *Surf. Coat. Technol.* **2013**, *235*, 108–116. [[CrossRef](#)]

41. Li, W.Y.; Zhang, G.; Liao, H.L.; Coddet, C. Characterizations of cold sprayed TiN particle reinforced Al2319 composite coating. *J. Mater. Process. Technol.* **2008**, *202*, 508–513. [[CrossRef](#)]
42. Wang, Q.; Spencer, K.; Birbilis, N.; Zhang, M.X. The influence of ceramic particles on bond strength of cold spray composite coatings on AZ91 alloy substrate. *Surf. Coat. Technol.* **2010**, *205*, 50–56. [[CrossRef](#)]
43. Shockley, J.; Descartes, S.; Vo, P.; Irissou, E.; Chromik, R. The influence of Al₂O₃ particle morphology on the coating formation and dry sliding wear behavior of cold sprayed Al–Al₂O₃ composites. *Surf. Coat. Technol.* **2015**, *270*, 324–333. [[CrossRef](#)]
44. Li, W.Y.; Zhang, G.; Zhang, C.; Elkedim, O.; Liao, H.; Coddet, C. Effect of ball milling of feedstock powder on microstructure and properties of TiN particle-reinforced Al alloy-based composites fabricated by cold spraying. *J. Therm. Spray Technol.* **2008**, *17*, 316–322. [[CrossRef](#)]
45. Yandouzi, M.; Bu, H.; Brochu, M.; Jodoin, B. Nanostructured al-based metal matrix composite coating production by pulsed gas dynamic spraying process. *J. Therm. Spray Technol.* **2012**, *21*, 609–619. [[CrossRef](#)]
46. Poirier, D.; Legoux, J.; Drew, R.; Gauvin, R. Consolidation of Al₂O₃/Al Nanocomposite Powder by Cold Spray. *J. Therm. Spray Technol.* **2011**, *20*, 275–284. [[CrossRef](#)]
47. Kang, K.; Bae, G.; Won, J.; Lee, C. Mechanical property enhancement of kinetic sprayed Al coatings reinforced by multi-walled carbon nanotubes. *Acta Mater.* **2012**, *60*, 5031–5039. [[CrossRef](#)]

Disclaimer/Publisher’s Note: The statements, opinions and data contained in all publications are solely those of the individual author(s) and contributor(s) and not of MDPI and/or the editor(s). MDPI and/or the editor(s) disclaim responsibility for any injury to people or property resulting from any ideas, methods, instructions or products referred to in the content.